International Journal of Environmental Sciences
ISSN: 2229-7359
Vol. 11 No. 24s, 2025
https://theaspd.com/index.php

Influence of Methanol Concentration on the Synthesis and Characteristics of Mesoporous Silica Nanoparticles: A DFT Reactivity Study

Mohammed M. Algaradah[1*]

[1*]Department of Chemistry, King Khalid Military Academy, Riyadh, Kingdom of Saudi Arabia.

***Corresponding Author:** Mohammed M. Algaradah
*Email: mohammed-chem@hotmail.com

Abstract

This study explores the synthesis and comprehensive characterization of mesoporous silica nanoparticles (MSNs), with particular emphasis on the influence of methanol concentration and its electronic reactivity, examined through density functional theory (DFT). A modified Stöber method was employed, using tetramethoxysilane (TMOS) as the silica precursor, methanol (Me-OH) as the solvent, and dodecyltrimethylammonium bromide (C_{12}TMABr) as the structure-directing agent. Systematic variations in the molar ratios of TMOS, deionized water (DI-W), sodium hydroxide (NaOH), and Me-OH were performed to elucidate their effects on particle formation. The resulting materials were characterized by Brunauer–Emmett–Teller (BET) surface area analysis, scanning electron microscopy (SEM), Fourier-transform infrared spectroscopy (FT-IR), and thermogravimetric analysis (TGA). DFT calculations provided molecular-level insight into the electron density distribution and local reactivity of the methanol–silica cluster. Specific carbon atoms (e.g., C8 and C13) were identified as reactive centers with high susceptibility to nucleophilic attack, highlighting methanol's role in modulating hydrolysis and condensation pathways. Experimentally, variations in precursor concentrations and reaction parameters produced nanoparticles with tunable diameters (100–1301 nm), pore sizes (1.01–4.42 nm), and surface areas (815–1159 $m^2.g^{-1}$). These findings advance the mechanistic understanding of mesoporous silica synthesis by linking reaction chemistry with structural outcomes. The demonstrated tunability of particle size, porosity, and surface area underscores the potential of MSNs for diverse applications, particularly in drug delivery and environmental remediation.

Keywords: *Nanoparticles, Mesoporous Silica, Methanol, Fourier-transform infrared spectroscopy (FT-IR), dodecyl trimethylammonium bromide (C_{12}TMABr)*

1- INTRODUCTION

The development of mesoporous silica commenced in 1992 when researchers successfully synthesized these materials utilizing surfactants as structure-directing agents [1]. The subsequent removal of surfactants from the mesostructured yielded silica materials characterized by pore sizes typically ranging from 2 to 10 nm, exhibiting hexagonal or cubic arrangements [2]. Since that time, extensive research has been devoted to tailoring mesoporous silica with diverse pore sizes and surface areas to accommodate various applications [3,4].

The preparation of mesoporous silica generally encompasses three critical stages: synthesis, drying, and surfactant removal [5]. The synthesis phase is particularly paramount, as it governs the final structural and morphological properties of the material. A meticulous selection of reactants is essential for achieving the desired characteristics [6]. During the drying phase, it is crucial to maintain temperatures below 45°C to facilitate the gradual removal of water and solvents while preventing the collapse of the mesostructured. The final stage involves the elimination of the surfactant template, typically accomplished through calcination or solvent extraction; however, these techniques exert limited influence over the regulation of pore size and surface area [7]. Despite significant advancements in the synthesis of mesoporous and macroporous silica materials, relatively few studies have successfully produced particles with an average diameter below 500 nm [8]. Mesoporous silica's structural properties are influenced by several parameters, including pore size, surface area, and shape, among others. The selection of the surfactant and the length of its chain, the kind of solvent and the concentration of the solvent, the pH of the reaction medium, and the conditions under which the stirring is performed are all included in these parameters. Previous research has proven that it is possible to produce mesoporous silica by applying alkyl trimethylammonium chloride surfactants with various chain lengths. The silica precursor that was used in these investigations was tetraethoxysilane (TEOS). Me-OH and DI-W have frequently been utilized as solvents, with NaOH

introduced to establish an alkaline reaction environment. The resulting particles exhibited a range of sizes, with larger particles correlating with longer alkyl chains. Additionally, surface modifications, such as functionalization with chelating agents, have been investigated to enhance specific applications.
Despite these advancements, challenges persist in the precise control of the shape, pore size, and surface area of mesoporous silica particles. The present study aims to address these challenges by systematically varying the molar concentration of TMOS and other reaction components, thereby achieving improved control over particle characteristics. This research specifically focuses on examining the impact of Me-OH concentration on the properties of the synthesized mesoporous silica.

2- METHODS AND MATERIALS

In this study, mesoporous silica was synthesized utilizing a variety of chemical reagents, specifically TMOS (98%), NaOH (98%), C_{12}TMABr (99%), Me-OH and ethanol (Et-OH). All chemicals were procured from Aldrich, UK. Me-OH and Et-OH functioned as grading agents throughout the synthesis process.

2.1 Characterization of Prepared Particles:

The characterization of the mesoporous silica particles synthesized in this study was conducted utilizing TGA, FT-IR, SEM, and BET surface area analysis. Thermal stability was evaluated using a Perkin-Elmer TGA 8000 instrument, wherein samples ranging from 1 to 5 mg were subjected to heating from 30°C to 800°C at a rate of 2°C per minute in a nitrogen atmosphere. FT-IR spectroscopy was employed to analyze the silica samples both prior to and after combustion, with measurements conducted in their solid state. The morphological characteristics and particle size distribution were assessed through SEM, with the average particle size determined based on measurements from 50 individual particles. For SEM analysis, 10 mg of silica particles were suspended in deionized water, and small aliquots of the suspension were deposited onto a glass substrate. The samples were subsequently coated with a thin layer of gold before imaging using a focused ion-beam microscope (FEI Helios Nanolab 600). The specific surface area and pore size distribution were evaluated using a Micromeritics ASAP 2020 analyzer.

2.2 Preparation of mesoporous silicas:

The synthesis process of mesoporous silica involved several critical steps. Initially, Me-OH (0–400 mL), DI-W (0–400 mL), NaOH solution (0–9 mL, 1M), and C_{12}TMABr (0–3.36 g) were combined in a 1000 mL conical flask. The resulting solution was vigorously stirred at 20°C for 15 minutes. Subsequently, TMOS (0.9–3.6 mL) was gradually introduced into the reaction mixture, which was continuously agitated for 8 hours, as detailed in Table 1. Following this, the reaction mixture was allowed to mature undisturbed overnight. The resultant white solid was isolated by centrifugation at 10,000 rpm for 30 minutes, followed by thorough washing five times with water and once with Et-OH. The sample was then dried at 45°C for a duration of three days. Finally, calcination was conducted at 550°C for 12 hours, with the temperature being incrementally raised from room temperature to 550°C at a controlled rate of 2°C per minute.

Table 1: The materials and quantities used to prepare different batches of mesoporous silicas:

Experiment	TMOS mL	C_{12}TMABr g	DI-W mL	Me-OH ml	NaOH mL
MG-1	1.8	1.69	310	90	3
MG-2	0.9	1.69	310	90	3
MG-3	3.6	1.69	310	90	3
MG-4	1.8	1.69	200	200	3
MG-5	1.8	1.69	90	310	3
MG-6	1.8	1.69	400	0	3
MG-7	1.8	1.69	0	400	3
MG-8	1.8	1.69	310	90	0
MG-9	1.8	1.69	310	90	6
MG-10	1.8	1.69	310	90	10
MG-11	1.8	0	310	90	3
MG-12	1.8	0.84	310	90	3
MG-13	1.8	3.36	310	90	3

*mL= milliliters, g=grams,

3- RESULTS AND DISCUSSION

3.1 Effect of tetramethoxysilane (TMOS)

In this investigation, TMOS was selected as the silica precursor in place of TEOS, which is more conventionally employed for mesoporous silica synthesis. The rationale for this substitution is grounded in the intrinsic reactivity of TMOS: the smaller methyl leaving group undergoes hydrolysis at a significantly faster rate compared to the ethyl group in TEOS. This enhanced hydrolysis kinetics promotes accelerated condensation, thereby facilitating the rapid nucleation and formation of silica nanoparticles [9]. For the structure-directing agent, cetyltrimethylammonium bromide with a 12-carbon chain length (C_{12}TMABr) was employed. Its relatively short hydrophobic tail was anticipated to produce smaller micellar templates, leading to the formation of mesostructured silica particles with reduced dimensions compared to templates with longer alkyl chains. Me-OH was selected as the solvent instead of ethanol or ethylene glycol. The choice of Me-OH was motivated by its lower viscosity and higher diffusivity, which together provide a less resistant reaction medium. In contrast, Et-OH and ethylene glycol generally increase the viscosity of the solution, thereby impeding mass transport and fostering the generation of a greater number of primary nuclei. This effect often yields particles with broader size distributions and less controllable morphologies [10]. In terms of catalyst selection, sodium hydroxide (NaOH) was utilized instead of ammonium hydroxide (NH_4OH), which is commonly employed in silica sol–gel systems. NaOH promotes the formation of short silicate rod-like micelles due to its stronger base strength and higher ionic concentration in solution. These structural features of the reaction medium are advantageous for reducing particle size by enhancing the packing density of the silica-surfactant assemblies [11].

Each reagent within the synthetic system played a pivotal role in dictating particle nucleation, growth, and structural evolution. To systematically interrogate these effects, the experimental design varied the concentrations of the silica precursor, surfactant, and solvent, while maintaining constant stirring and temperature conditions (Table 1). The resulting mesoporous silica particles were then characterized in terms of morphology, particle size, specific surface area, and pore size distribution. A key focus was the influence of precursor concentration on particle formation. Initial experiments employed varying amounts of TMOS, which were gradually increased to assess how precursor availability modulates nucleation and growth dynamics.

The systematic variation of TMOS concentration demonstrated its critical role in controlling particle characteristics. At a moderate precursor volume (Batch MG-1, 1.8 mL TMOS), the reaction produced highly monodisperse spherical nanoparticles with an average diameter of 156 ± 21 nm, reflecting an optimal balance between hydrolysis and condensation that enabled well-regulated nucleation and growth. When the TMOS concentration was reduced by 50% (Batch MG-2, 0.9 mL), the precursor supply became insufficient to sustain uniform nucleation, leading to the aggregation of smaller nuclei and the formation of substantially larger particles with an average diameter of 286 ± 24 nm, accompanied by slightly diminished uniformity. Conversely, increasing the TMOS concentration to 3.6 mL (Batch MG-3) promoted the initial growth of spherical particles with a mean diameter of 357 ± 21 nm. However, at elevated precursor levels, the accelerated hydrolysis triggered excessive nucleation, generating a high density of seed particles that competed for the available silica source. This competition restricted subsequent growth, ultimately reducing the final particle size to approximately 200 nm in later high-concentration batches (Table 1).

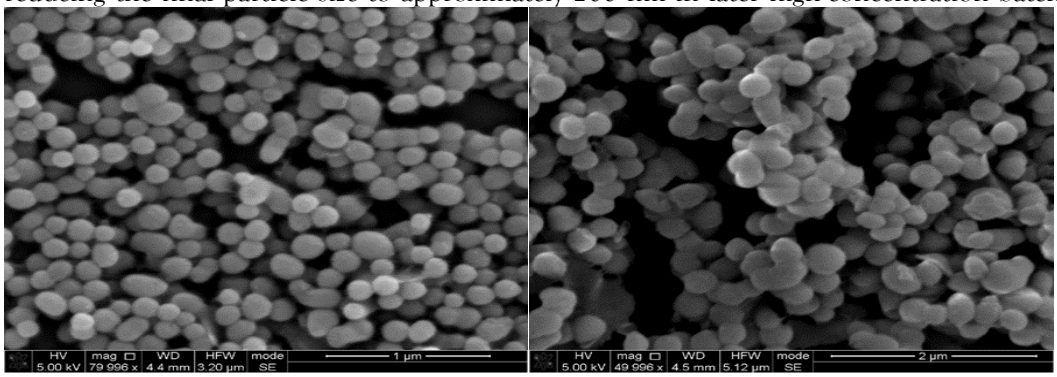

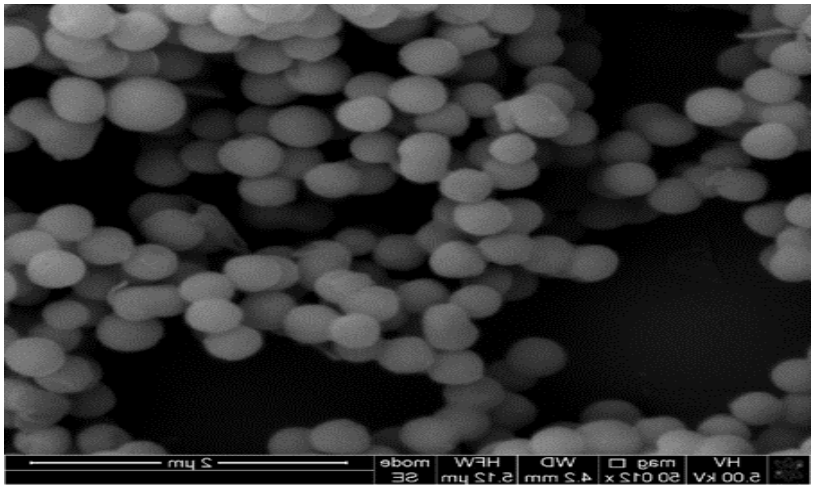

Figure 1: SEM image of silica particles prepared by altering the quantity of TMOS (Batch MG-1 to MG-3)

3.2 Effect of volume ratio of solvent (DI-W: Me-OH)

This study systematically investigated the effect of solvent composition—specifically the ratio of DI-W to MeOH on the size, morphology, and structural uniformity of mesoporous silica particles. Each batch was synthesized with a fixed total solvent volume of 400 mL, while the DI-W/MeOH ratio was varied across batches MG-1 and MG-4 to MG-7 to elucidate solvent-dependent trends in particle formation. For instance, batch MG-1 was prepared with 310 mL of DI-W and 90 mL of MeOH, serving as a baseline composition for subsequent comparisons.

Morphological and dimensional analyses revealed that progressive enrichment of MeOH in the reaction medium exerted a marked influence on particle characteristics (Figure 2). Increasing the fraction of MeOH altered the physicochemical environment of the surfactant–solvent system, thereby affecting micelle stability and the condensation dynamics of hydrolyzed silicate species. At moderate MeOH concentrations, a partial reduction in surfactant solubility was observed, which impaired the cooperative organization of surfactant micelles. This destabilization translated into less uniform templating, thereby producing particles with broader size distributions and irregular surface features.

At higher MeOH content, these effects became more pronounced. The solvent's lower polarity and lower hydrogen-bonding capacity relative to water significantly decreased surfactant solubility, leading to the disruption of micellar packing and ultimately preventing the formation of ordered mesostructures. In batch MG-7, where MeOH dominated the solvent system, spherical particle formation was entirely suppressed, and the resulting products lacked any discernible mesostructural order. This outcome highlights the essential role of DI-W in maintaining micellar integrity and facilitating the cooperative self-assembly of silica around surfactant templates.

Overall, the experimental results demonstrate that solvent composition is a decisive factor in controlling both particle size and morphology. While moderate proportions of MeOH can fine-tune particle dimensions, excessive MeOH disrupts the micellar templating process and compromises structural organization. The measured particle sizes and key physicochemical properties of the synthesized samples are summarized in Table 2 [14], providing quantitative evidence for these solvent-dependent effects.

Table 2: Some characteristics for different batches of mesoporous silicas

Batch	Main Change on the Reaction content	Particles size ± SD (nm)	Dispersion of the particles	Characteristics of the particles
MG-1	TMOS = 1.8 mL	156 ± 21	Good dispersion	Spherical particles
MG-2	TMOS = 0.9 mL	286 ± 24	Good dispersion	Spherical particles
MG-3	TMOS = 3.6 mL	357 ± 21	Good dispersion	Spherical particles
MG-4	DI-W: Me-OH = (200: 200) mL	1301 ± 238	Poor dispersion	Spherical particles, some amorphous sheet
MG-5	DI-W: Me-OH = (90: 310) mL	435 ± 10	Poor dispersion	Spherical particles, some amorphous sheet

MG-6	DI-W: Me-OH = (400: 0) mL	100 ± 24	Reasonable dispersion	Spherical particles, some amorphous sheet
MG-7	DI-W: Me-OH = (0: 400) mL	No product		
MG-8	NaOH = 0 mL	No product		
MG-9	NaOH = 6 mL	377 ± 84	Reasonable dispersion	Spherical particles, some spherical particles with Irregular shape
MG-10	NaOH = 10 mL	448 ± 76	Reasonable dispersion	Spherical particles, some spherical particles with Irregular shape
MG-11	C_{12}MABr = 0 g	Glass solid	No dispersion	
MG-12	C_{12}MABr = 0.84 g	631 ± 96	Very Good dispersion	Very Good spherical shape particles
MG-13	C_{12}MABr = 3.36 g	107 ± 5	Very Good dispersion	Very Good spherical shape particles

*mL= milliliters, g=grams

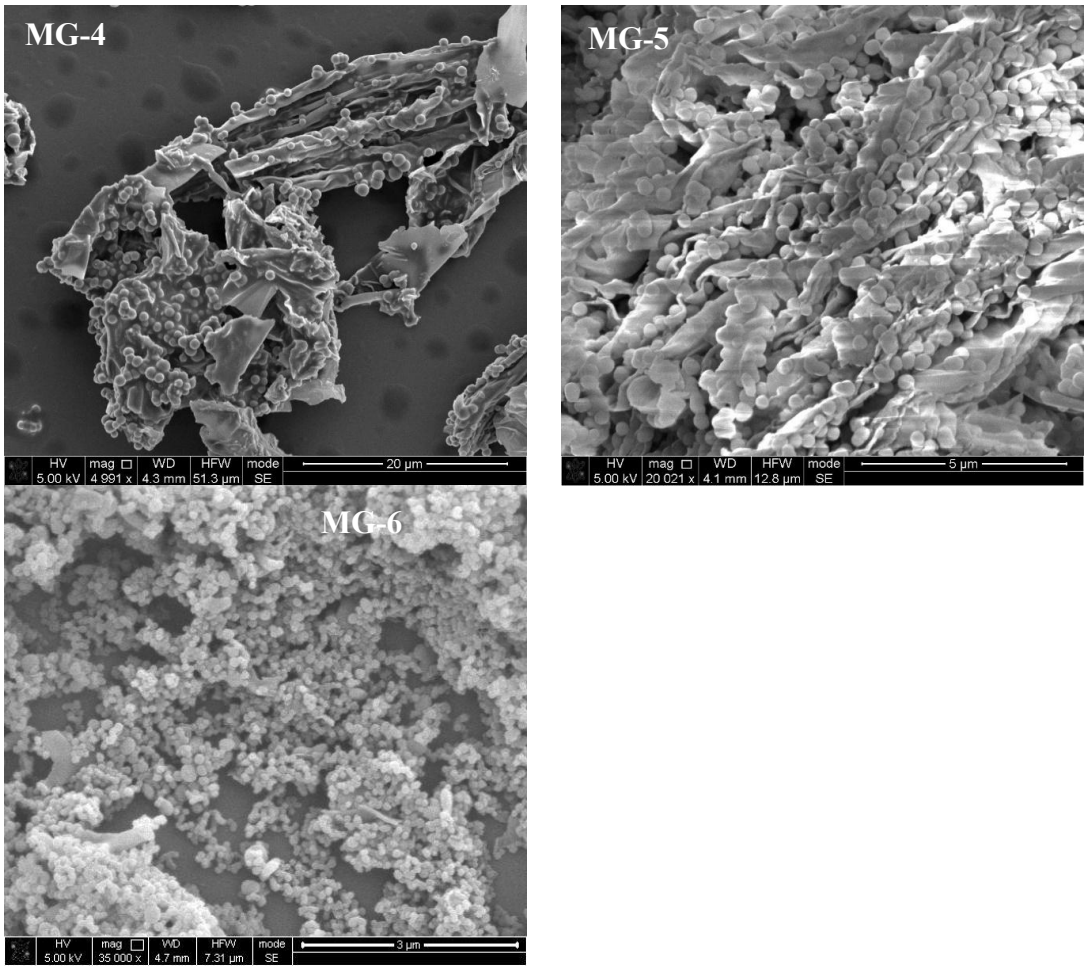

Figure 2: SEM image silica particles (Batch MG-4,5,6)

3.3 Alkaline Reagent (Sodium Hydroxide):

The influence of NaOH as an alkaline catalyst on mesoporous silica synthesis was systematically evaluated in batches MG-1 and MG-8 to MG-10, with NaOH concentrations varied between 0 and 9 mL. The catalytic role of NaOH arises from its ability to generate hydroxide ions (OH^-), which accelerate the hydrolysis of the silica precursor (TMOS) and subsequently promote condensation into siloxane (Si–O–Si) frameworks. The effect of catalyst concentration on particle morphology and size distribution provides important mechanistic insights into the sol–gel process.

In the absence of NaOH (batch MG-8), no discernible nanoparticles were obtained. Instead, the reaction yielded an amorphous, glass-like solid, underscoring the requirement for a controlled acidic or alkaline environment to initiate hydrolysis–condensation reactions. Without sufficient OH^- ions, hydrolysis of TMOS proceeds too slowly to support the cooperative assembly of silica around the surfactant micelles, resulting in non-particulate amorphous material (Table 2).

Upon the introduction of NaOH, the reaction medium underwent a substantial pH increase, which enhanced the rate of precursor hydrolysis and condensation. At moderate NaOH concentrations (e.g., batch MG-1), these conditions facilitated the formation of uniform, spherical nanoparticles, reflecting a favorable balance between nucleation and growth kinetics. However, further increases in NaOH concentration disrupted this balance. At high catalyst loadings (batch MG-10, 9 mL NaOH), excessive OH^- accelerated hydrolysis to such an extent that an abundance of silanol groups formed rapidly, leading to uncontrolled and simultaneous nucleation events. The subsequent condensation of these nuclei produced irregular aggregates, yielding particles with larger average diameters, heterogeneous size distributions, and non-spherical morphologies, as evidenced by scanning electron microscopy (Figure 3) [15].

These observations highlight that while the presence of NaOH is essential for initiating nanoparticle formation, its concentration must be carefully optimized. Too little catalyst suppresses hydrolysis altogether, while excessive catalyst induces uncontrolled nucleation and structural disorder. Thus, the role of NaOH is not only catalytic but also regulatory, governing the delicate balance between precursor hydrolysis, silicate condensation, and surfactant-templated particle organization.

.

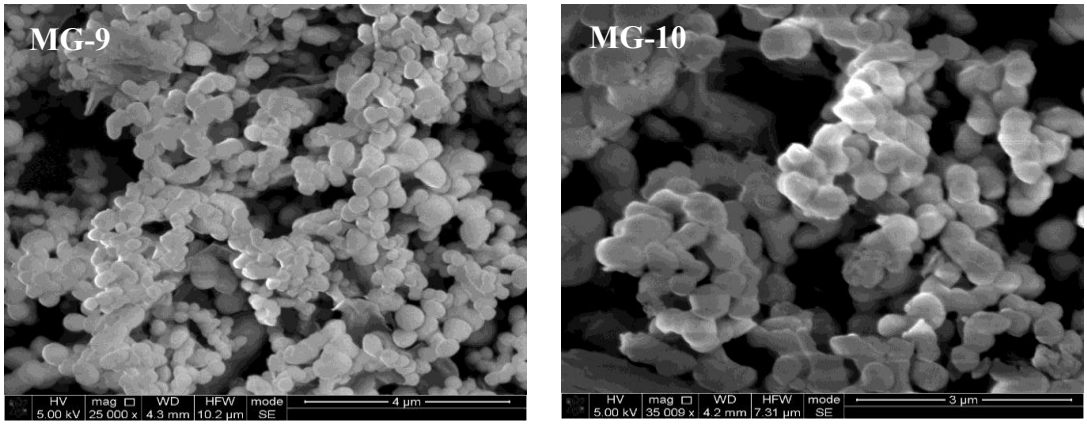

Figure 3: SEM image of mesoporous silica particles (Batch MG-9 and 10)

3.4 Template dodecyl trimethylammonium bromide (C_{12}TMABr)

Particle size and morphology in mesoporous silica systems are strongly dependent on the characteristics of the surfactant template. Prior studies have established that increasing the alkyl chain length of surfactants generally correlates with the formation of larger silica particles, owing to the expansion of micellar dimensions and the corresponding enlargement of templated pores [16]. While this chain length effect is relatively well documented, the influence of surfactant concentration on particle formation remains less thoroughly understood, particularly in the context of balancing nucleation and growth dynamics.

In the present work, the role of the surfactant cetyltrimethylammonium bromide (C_{12}TMABr) was systematically investigated. In the absence of surfactant (batch MG-11), no ordered mesostructure was observed; instead, the reaction produced an amorphous, glass-like solid (Table 2). This outcome highlights the indispensable role of C_{12}TMABr as a structure-directing agent, facilitating cooperative self-assembly of silica species into well-organized, spherical nanoparticles. Without micelle formation, hydrolyzed silicate species condense randomly, leading to non-particulate amorphous networks rather than discrete nanostructures.

When surfactant concentration was increased, a pronounced reduction in particle size was observed. At high concentrations of C_{12}TMABr (batch MG-13), spherical nanoparticles with an average diameter of 107 ± 5 nm were obtained. This reduction in particle size can be attributed to the increased number of micelles available to act as nucleation sites. The higher micelle density disperses the hydrolyzed silicate species among a larger number of nucleating centers, thereby limiting the growth of individual particles and yielding smaller, more uniform nanoparticles.

By contrast, at lower surfactant concentrations, fewer micelles were available to template the silica framework, resulting in fewer nucleation sites and more precursor available for growth around each micelle. This produced larger spherical particles, which nevertheless displayed improved dispersion stability and more well-defined morphologies compared to surfactant-free conditions (Figures 1 and 4). These findings underscore that surfactant concentration exerts a dual influence: while higher concentrations favor smaller, uniform nanoparticles, moderate concentrations can yield larger but well-dispersed spheres with structurally coherent mesoporosity.

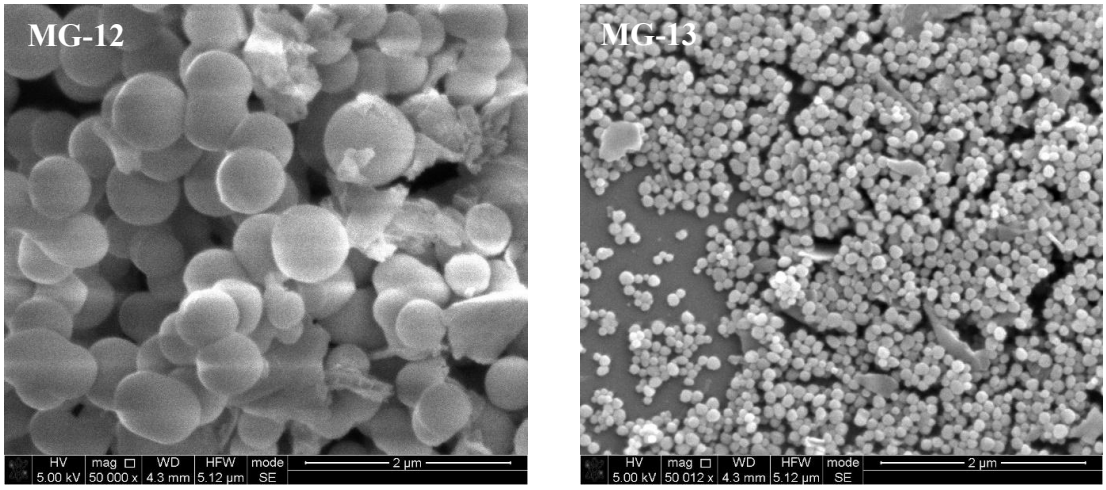

Figure 4: SEM image of mesoporous silica particles (Batch MG-12 and 13)

3.5 Surface area and pore size distribution

The porosity of the synthesized silica particles was systematically characterized using nitrogen (N_2) adsorption–desorption isotherms, with specific surface area and pore size distribution calculated according to the BET method [17]. Across all experimental batches, the adsorption profiles displayed type IV isotherms with distinct hysteresis loops, a signature feature of mesoporous materials [18]. These findings confirm that the synthetic strategy successfully produced mesostructured silica with interconnected mesopores, consistent with the templating effect of the C_{12}TMABr surfactant.

Quantitative analysis revealed that reagent concentration strongly modulated both surface area and pore architecture. The measured BET surface areas ranged from 815 to 1159 $\mathbf{m^2\ g^{-1}}$, while the average pore radii varied between 1.01 and 4.42 **nm** (Table 3). Notably, solvent composition exerted a pronounced effect: when equal volumes of DI-W and Me-OH (200 mL each) were employed, the resulting particles exhibited a reduction in surface area relative to solvent systems dominated by either DI-W or Me-OH. This suggests that the balance between hydrolysis (favored by DI-W) and micelle organization (modulated by Me-OH) was disrupted at the equimolar solvent ratio, leading to less efficient pore templating and reduced accessible surface area. By contrast, when the solvent system was enriched in either DI-W or Me-OH, improved pore organization and higher surface areas were observed, indicating that asymmetric solvent compositions provide more favorable conditions for micelle–silicate interactions.

Further trends indicated a strong positive correlation between the amount of DI-W and the specific surface area of the resulting silica, implying that enhanced hydrolysis and more complete silanol condensation promote the development of highly porous frameworks. Interestingly, the pH of the reaction medium, which was varied through NaOH addition, exhibited no measurable influence on either surface area or pore size within the investigated range. This finding suggests that once hydrolysis is sufficiently activated, surfactant organization and solvent composition become the dominant factors governing pore architecture.

The effect of surfactant concentration was particularly pronounced. Increasing the concentration of C_{12}TMABr significantly enhanced surface area, consistent with its role in directing mesopore formation. A higher surfactant-to-silica ratio increases the density of micelles within the reaction medium, thereby providing a larger number of templating domains. This translates into a greater proportion of mesoporous volume and, consequently, higher accessible surface area. The data thus confirm that surfactant content is a critical lever for tailoring porosity, enabling fine control over both textural properties and functional performance of the synthesized mesoporous silica (Table 3).

Table 3: Surface area and BJH pore radius and total prepared mesoporous silica

Batch	Main Change on the Reaction content	BET Surface area "$m^2 \cdot g^{-1}$"	BJH Desorption average pore radius (2V/A) "nm"
MG-1	TMOS = 1.8 mL	1119.7729	2.1444
MG-2	TMOS = 0.9 mL	894.6002	2.7910
MG-3	TMOS = 3.6 mL	942.4271	2.2733
MG-4	DI-W: Me-OH = (200: 200) mL	815.9158	3.0307
MG-5	DI-W: Me-OH = (90: 310) mL	928.8079	2.1748
MG-6	DI-W: Me-OH = (400: 0) mL	1095.2449	1.6901
MG-7	DI-W: Me-OH = (0: 400) mL	1169.3896	1.0077
MG-8	NaOH = 0 mL	1002.3354	2.0953
MG-9	NaOH = 6 mL	1100.023	1.1254
MG-10	NaOH = 10 mL	1083.1221	1.7772
MG-11	C_{12}TMABr = 0 g		
MG-12	C_{12}TMABr = 0.84 g	819.1427	2.7306
MG-13	C_{12}TMABr = 3.36 g	1159.8091	4.4199

*mL= milliliters, g=grams

3.6 DFT-Based Reactivity Analysis

To elucidate the influence of methanol concentration on the nucleation and growth behavior of mesoporous silica particles (Figure 5), DFT calculations were performed to evaluate the electron density distribution and local reactivity of key atoms within a representative methanol–silica cluster. Fukui functions (f^+ and f^-), which describe susceptibility to electrophilic and nucleophilic attack, were derived from Hirshfeld charges computed at the B3LYP/6-31G(d) level using Gaussian 16. The calculated values are summarized in Table 4. The results revealed that specific carbon atoms, such as C13 and C8, displayed elevated f^+ values (0.0856 and 0.1138, respectively), identifying them as potential sites for nucleophilic attack. These sites are chemically activated by the polar environment of methanol, thereby facilitating silica hydrolysis and condensation reactions. In contrast, atoms such as C4 and N20 exhibited higher f^- values (0.0296 and 0.0995), indicating susceptibility to electrophilic attack by species such as H^+ or H_2O. These computational findings are consistent with the experimental observations, suggesting that methanol concentration modulates local electronic environments, thereby controlling particle size, morphology, and porosity.

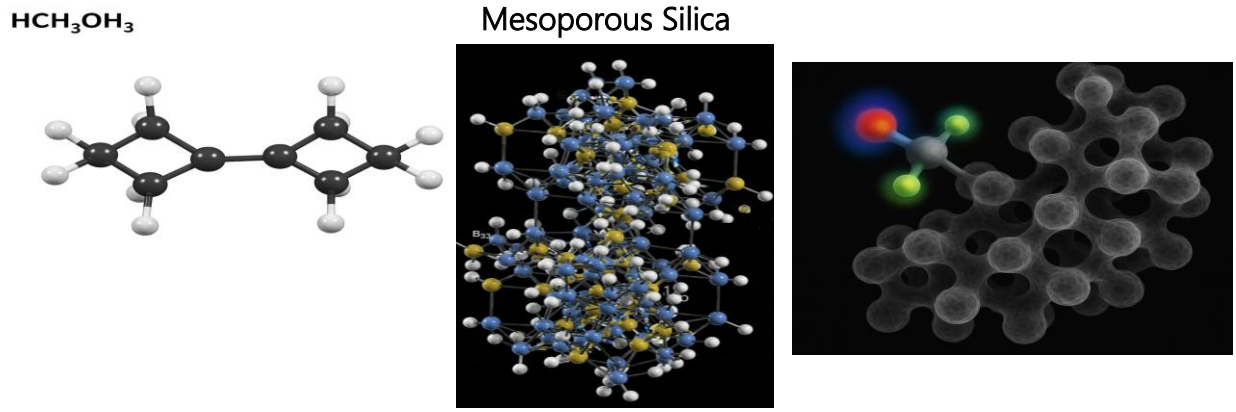

Figure 5: Molecular structure highlighting a methanol molecule (colored red, green, and yellow) interacting with a mesoporous silica framework

Table 4: Fukui function indices for nucleophilic (f^+) and electrophilic (f^-) attacks, calculated using Hirshfeld charge analysis for a methanol–silica precursor molecular model. Highlighted cells indicate the atoms with highest reactivity toward electrophilic and nucleophilic species.

No.	Atom	q(N)	q(N+1)	q(N−1)	f^-	f^+
1	C	-0.0763	-0.0848	-0.0685	0.0078	0.0085

2	C	0.037	0.0303	0.0411	0.0042	0.0067
3	C	0.0352	0.0324	0.0442	0.0050	0.0068
4	C	-0.1269	-0.1519	-0.0973	**0.0296**	0.0148
5	C	-0.0012	-0.0076	-0.0021	0.0016	**0.0474**
6	C	-0.0195	-0.0162	-0.0351	0.0156	0.0079
7	C	-0.0361	-0.0492	-0.0505	0.0076	**0.0358**
8	C	-0.0347	-0.0792	-0.0523	0.0176	**0.1138**
9	C	-0.0595	-0.1002	-0.1005	0.0206	**0.0407**
10	C	0.1972	0.1685	0.2854	0.0144	0.0287
11	C	-0.0103	-0.0089	-0.0136	0.0017	0.0033
12	C	-0.2705	-0.326	-0.2363	0.0317	**0.0656**
13	C	-0.2705	-0.3536	-0.2317	**0.0393**	**0.0856**
14	C	-0.1296	-0.1802	-0.1033	0.0263	**0.0546**
15	C	-0.0297	-0.0351	-0.021	0.0079	0.0073
16	C	0.0511	0.0359	0.0893	0.0182	**0.0498**
17	C	-0.081	-0.1169	-0.0703	0.0107	0.0234
18	F	-0.0946	-0.1269	-0.0783	0.0202	0.0323
19	C	0.026	0.0196	0.0346	0.0084	0.0074
20	N	-0.0955	-0.0929	-0.1097	**0.0068**	**0.0995**
21	C	0.0226	0.0186	0.0355	0.0129	0.0040
22	C	-0.0011	-0.005	0.0024	0.0013	0.0062
23	C	0.035	0.0306	0.0444	0.0094	0.0044
24	C	-0.0411	-0.0615	-0.0325	0.0145	0.0058
25	C	0.0012	-0.0166	0.0086	0.0148	0.0033
26	C	-0.0087	-0.0125	-0.0092	0.0018	0.0035

*q(N) = charge in the neutral state, q(N+1) = charge after accepting one electron, q(N−1) = charge after losing one electron, f^+ = Fukui function for nucleophilic attack, and f^- = Fukui function for electrophilic attack. (overall reactivity: + = electrophilic, – = nucleophilic)

Complementary to the Fukui function analysis, the electronic structure of the methanol–silica cluster was further characterized through highest occupied molecular orbital (HOMO), lowest unoccupied molecular orbital (LUMO), and electrostatic potential (ESP) mapping, computed using the same DFT level of theory (B3LYP/6-31G(d)). The orbital isosurfaces (Panels a and b) illustrate the spatial electron density distribution of the frontier orbitals, while the ESP map (Panel c) highlights the electrostatic landscape of the molecular surface. The HOMO, primarily localized on oxygen-containing functional groups and methanol molecules, indicates their role as electron donors during hydrolysis and condensation (Figure 6a). Conversely, the LUMO was predominantly distributed over the silicon centers and adjacent framework regions, identifying these as electron-acceptor sites (Figure 6b). The ESP surface further supported this assignment, with electron-rich regions (red) localized around electronegative oxygen atoms and electron-deficient regions (blue) concentrated near silicon atoms (Figure 6c). Together, these analyses provide strong evidence that methanol contributes directly to the electronic activation and stabilization of reactive sites within the silica precursor system, thereby governing nucleation and growth pathways.

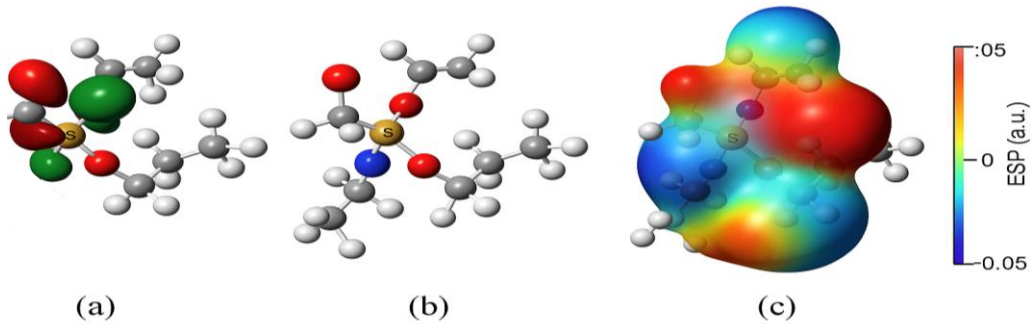

Figure 6: (a) HOMO and (b) LUMO orbital isosurfaces of a methanol–silica molecular cluster obtained at the B3LYP/6-31G(d) level, showing electron density distribution in donor and acceptor regions. (c)

Electrostatic potential (ESP) map visualized on the van der Waals surface. Red areas indicate regions of negative potential (electron-rich), while blue areas represent positive potential (electron-deficient), supporting the reactive site predictions from Fukui function analysis

3.7 Template removal

The removal of surfactant templates from mesoporous silica is a critical step in generating accessible pore channels and enhancing surface functionality. This process is conventionally achieved either by thermal combustion (calcination) or by solvent extraction. Calcination, when performed at moderate temperatures (≤600 °C), is considered a straightforward, cost-effective, and environmentally favorable approach, as it circumvents the use of organic solvents and minimizes chemical waste. However, exposure to excessively high temperatures (>600 °C) can induce partial or complete structural collapse of the mesoporous framework, resulting in pore shrinkage, reduction in surface area, and damage to the overall nanoparticle architecture. Therefore, optimization of calcination conditions is essential to ensure efficient surfactant removal while preserving mesostructural integrity.

In this study, the efficiency of template elimination was systematically investigated using TGA and FT-IR. These complementary techniques were applied to particles obtained from multiple batches, both in their as-synthesized (surfactant-containing) state and after calcination. TGA measurements were conducted over a temperature range of 30–800 °C, enabling identification of distinct weight-loss events associated with solvent evaporation, surfactant decomposition, and framework stabilization.

The TGA profiles consistently exhibited three sequential stages of weight loss. The first stage, occurring between 40 and 180 °C, was attributed to the evaporation of physically adsorbed water molecules and residual unreacted solvents confined within the silica matrix [19]. This was followed by a pronounced weight-loss event in the range of 180–350 °C, corresponding to the oxidative thermal decomposition of the organic surfactant template (C_{12}TMABr). The sharp decline in mass during this stage is characteristic of surfactant removal and is commonly associated with the breakdown of alkyl chain segments. A subsequent, smaller mass reduction between 350 and 420 °C was observed, likely associated with the elimination of residual carbonaceous fragments or further oxidative degradation of partially decomposed organic moieties. Beyond 420 °C, no significant changes in mass were detected up to 800 °C, indicating the thermal stability of the silica framework once template removal was complete.

Crucially, the absence of a pronounced weight-loss step between 180 and 350 °C in the post-calcination TGA profiles confirmed the complete removal of the surfactant template from the silica framework (Figure 8). These results were further corroborated by FT-IR spectra, which showed the disappearance of characteristic C–H stretching vibrations associated with surfactant alkyl chains in calcined samples, confirming the successful generation of clean, mesoporous silica networks. Together, these analyses demonstrate that calcination under controlled thermal conditions effectively eliminates the surfactant while preserving the mesostructural order of the nanoparticles, thereby producing stable mesoporous silica suitable for advanced applications.

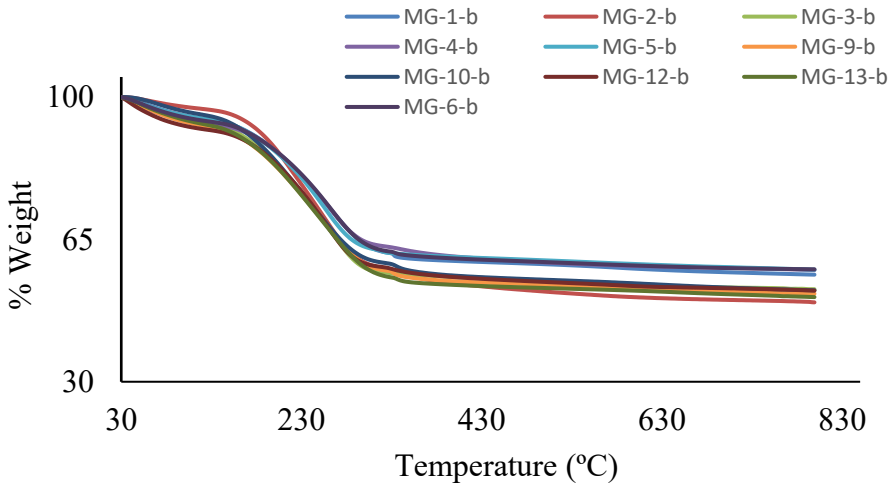

Figure 7: Thermogravimetric analysis of mesoporous silicas before burning of surfactant

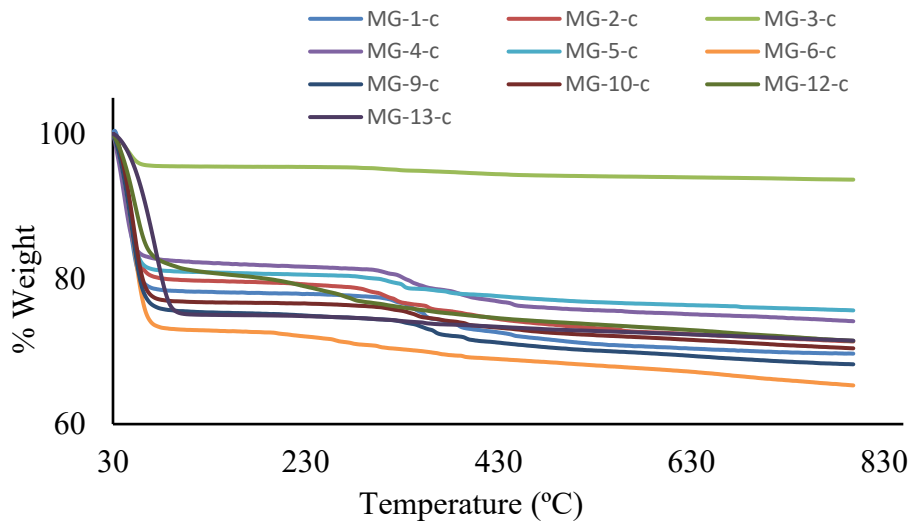

Figure 8: Thermogravimetric analysis of mesoporous silicas after burning of surfactant

FT-IR spectroscopy was employed as a complementary technique to validate the removal of surfactant molecules from the mesoporous silica framework. Spectra were recorded for representative samples both before and after calcination, enabling direct comparison of organic and inorganic vibrational features associated with the template and the silica network, respectively.

In the pre-calcination spectra (Figure 10), distinct absorption bands were observed at 2925 cm^{-1} and 2851 cm^{-1}, corresponding to the asymmetric and symmetric stretching modes of aliphatic CH_2 and CH_3 groups, respectively. These bands are characteristic signatures of the long alkyl chains in the C_{12}TMABr surfactant, confirming its incorporation within the silica matrix during synthesis. The intensity of these bands served as an indicator of surfactant loading, with stronger peaks reflecting higher concentrations of organic template entrapped within the pores.

Following thermal calcination, these hydrocarbon-related bands were absent in most batches (Figure 9), confirming the efficient removal of surfactant molecules and associated organic residues from the mesoporous network. The disappearance of C–H stretching vibrations demonstrates that combustion successfully eliminated the alkyl chains of C_{12}TMABr, leaving behind a clean silica framework with accessible pore channels. However, in certain batches, weak residual peaks persisted at 2925 and 2851 cm^{-1}. These features likely arise from incomplete surfactant removal or from strongly adsorbed carbonaceous fragments trapped within narrow pore channels, where diffusion of combustion byproducts is kinetically hindered. This batch-to-batch variability underscores the sensitivity of template removal efficiency to calcination parameters such as heating rate, dwell time, and airflow.

Beyond the C–H stretching region, the post-calcination spectra exhibited the well-defined fingerprint of the silica network. A strong, broad absorption band centered around 1036 cm^{-1} was assigned to the asymmetric stretching vibrations of Si–O–Si linkages, while a smaller band at 791 cm^{-1} corresponded to the symmetric stretching of Si–O bonds. In addition, a weak band near 962 cm^{-1} was occasionally detected, which can be attributed to terminal Si–OH stretching vibrations, reflecting the presence of residual silanol groups on the particle surface. The persistence of these characteristic silica bands confirmed that the mesostructural integrity of the framework was preserved during calcination, despite the high temperatures employed for surfactant removal.

Overall, the FT-IR analysis corroborates the TGA findings, demonstrating that calcination effectively removes the organic template while retaining the structural order of the silica matrix. The occasional detection of residual organic bands highlights the need for careful optimization of calcination conditions to ensure complete surfactant elimination and reproducibility across different synthesis batches.

International Journal of Environmental Sciences
ISSN: 2229-7359
Vol. 11 No. 24s, 2025
https://theaspd.com/index.php

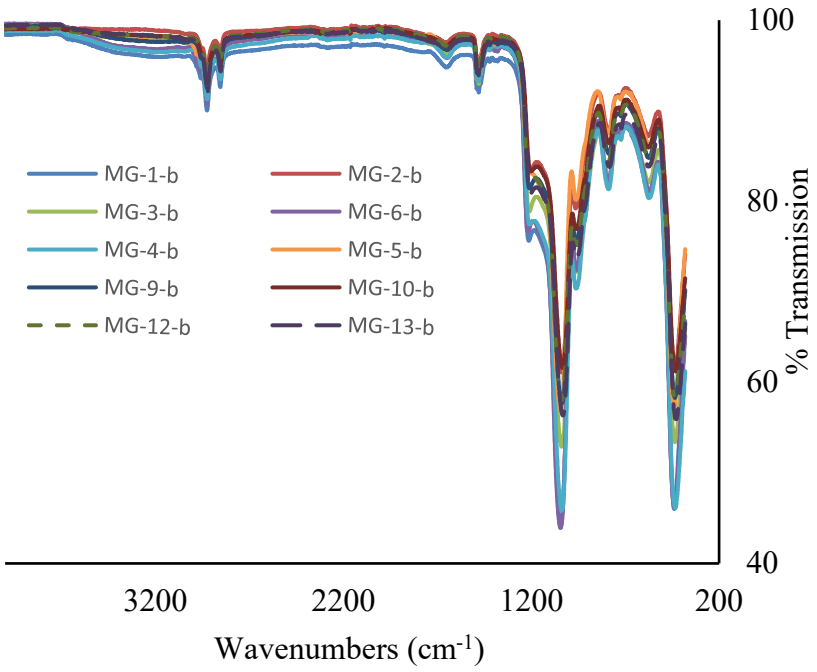

Figure 9: FT-IR spectroscopy of prepared mesoporous silicas before surfactant combustion

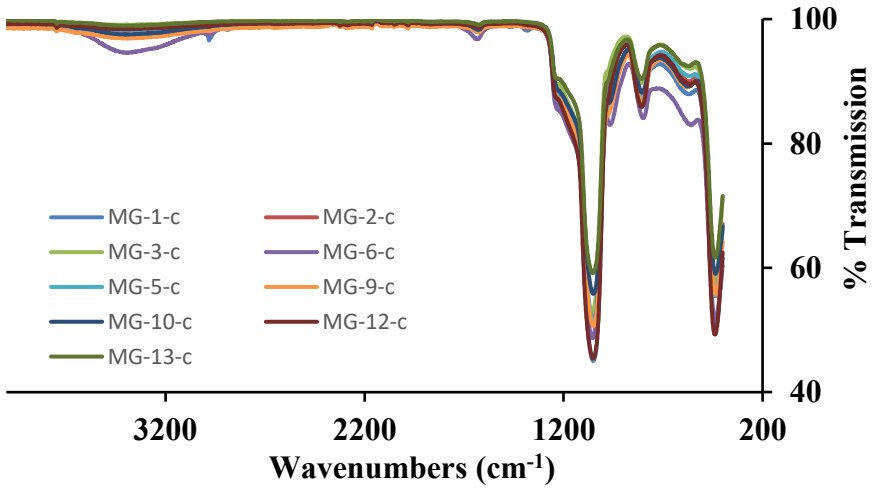

Figure 10: FT-IR spectroscopy of prepared mesoporous silicas after surfactant combustion

4- CONCLUSIONS

This study demonstrates that precise modulation of reagent concentrations during the synthesis of mesoporous silica particles exerts a profound effect on their structural and physicochemical properties, including morphology, particle size distribution, porosity, and surface area. The variations observed were primarily governed by the amount of TMOS precursor, the ratio of DI-W to Me-OH, and the concentrations of NaOH and C_{12}TMABr. These findings underscore the critical role of reaction stoichiometry and solvent environment in directing both nucleation and growth processes, thereby enabling the rational design of silica nanoparticles with tailored characteristics. Complementary density functional theory (DFT) calculations provided mechanistic insights at the molecular scale, revealing electron density distribution and local reactivity within the methanol–silica cluster. The analysis identified specific carbon atoms (e.g., C8 and C13) as nucleophilic hotspots, strongly susceptible to electron attack, while oxygen and silicon centers

acted as electron donors and acceptors, respectively. These results suggest that methanol not only modulates the solvent environment but also actively participates in hydrolysis and condensation reactions through electronic activation of reactive centers.

Experimentally, the systematic variation of reagents yielded silica particles with diameters ranging from 100 to 1301 nm, pore radii between 1.01 and 4.42 nm, and surface areas from 815 to 1159 $m^2 g^{-1}$. Such tunability highlights the potential to design mesoporous silica tailored for specific applications, including controlled drug delivery, catalysis, and environmental remediation of hazardous contaminants.

Overall, this research establishes a direct correlation between synthesis parameters, electronic reactivity, and particle architecture. While these results provide a strong foundation, further investigations are warranted to explore the role of alternative solvents, surfactants with varying chain lengths, and multi-component templating strategies. Such studies will deepen the mechanistic understanding of mesoporous silica formation and broaden their applicability across advanced biomedical and environmental technologies.

Acknowledgements

The authors would like to acknowledge the help and support received from King Khalid Military Academy, National Guard, Saudi Arabia.

REFERENCES

[1] O.B. Pagar, H.S. Nagare, Y.M. Chine, R.R. Autade, P.R. Narode, V.M. Sanklecha, Mesoporous Silica: A Review, International Journal of Pharmaceutics and Drug Analysis, (2018) 1-12.
[2] C. Ottone, O. Romero, P. Urrutia, C. Bernal, A. Illanes, L. Wilson, Enzyme Biocatalysis and Sustainability, in: M. Piumetti, S. Bensaid (Eds.) Nanostructured Catalysts for Environmental Applications, Springer International Publishing, Cham, 2021, pp. 383-413.
[3] D.P. Ferris, P.R. McGonigal, L.S. Witus, T. Kawaji, M.M. Algaradah, A.R. Alnajadah, M.S. Nassar, J.F. Stoddart, Oxime Ligation on the Surface of Mesoporous Silica Nanoparticles, Organic Letters, 17 (2015) 2146-2149.
[4] C.F. Blanford, H. Yan, R.C. Schroden, M. Al-Daous, A. Stein, Gems of Chemistry and Physics: Macroporous Metal Oxides with 3D Order, Advanced Materials, 13 (2001) 401-407.
[5] M. Algaradah, A mercapto based nanoscavenger as promising tool for the dispersion preconcentration of trace elements in contaminated waters, Egyptian Journal of Chemistry, (2022) -.
[6] M.K. Liudmyla Karachevtseva, Bo Wang, Oleg Lytvynenko, Yurii Sementsov., Nanocoatings on 2D Macroporous Silicon Structures, Journal of Materials Science and Chemical Engineering, 7 (2019) 12-20.
[7] Y. Duan, X. Zhao, M. Sun, H. Hao, Research Advances in the Synthesis, Application, Assembly, and Calculation of Janus Materials, Industrial & Engineering Chemistry Research, 60 (2021) 1071-1095.
[8] J. Kobryń, J. Dałek, W. Musiał, The Influence of Selected Factors on the Aqueous Cryptotanshinone Solubility, Pharmaceutics, 13 (2021) 992.
[9] A.A. Issa, A.S. Luyt, Kinetics of Alkoxysilanes and Organoalkoxysilanes Polymerization: A Review, Polymers, 11 (2019) 537.
[10] O.A. El Seoud, N. Keppeler, N.I. Malek, P.D. Galgano, Ionic Liquid-Based Surfactants: Recent Advances in Their Syntheses, Solution Properties, and Applications, Polymers, 13 (2021) 1100.
[11] R. Narayan, U.Y. Nayak, A.M. Raichur, S. Garg, Mesoporous Silica Nanoparticles: A Comprehensive Review on Synthesis and Recent Advances, Pharmaceutics, 10 (2018).
[12] T. Hara, S. Makino, Y. Watanabe, T. Ikegami, K. Cabrera, B. Smarsly, N. Tanaka, The performance of hybrid monolithic silica capillary columns prepared by changing feed ratios of tetramethoxysilane and methyltrimethoxysilane, Journal of Chromatography A, 1217 (2010) 89-98.
[13] M. Cadrazco, A. Santamaría, I.C. Jaramillo, K. Kaur, K.E. Kelly, J.R. Agudelo, Characterization of renewable diesel particulate matter gathered from non-premixed and partially premixed flame burners and from a diesel engine, Combustion and Flame, 214 (2020) 65-79.
[14] P. Zarrintaj, J.D. Ramsey, A. Samadi, Z. Atoufi, M.K. Yazdi, M.R. Ganjali, L.M. Amirabad, E. Zangene, M. Farokhi, K. Formela, M.R. Saeb, M. Mozafari, S. Thomas, Poloxamer: A versatile tri-block copolymer for biomedical applications, Acta Biomaterialia, 110 (2020) 37-67.
[15] L. Hong-Ping, T. Chih-Pin, Synthesis of Mesoporous Silica Nanoparticles from a Low-concentration CnTMAX–Sodium Silicate Components, Chemistry Letters, 32 (2003) 1092-1093.
[16] K. Yano, Y. Fukushima, Synthesis of mono-dispersed mesoporous silica spheres with highly ordered hexagonal regularity using conventional alkyltrimethylammonium halide as a surfactant, Journal of Materials Chemistry, 14 (2004) 1579-1584.
[17] S. Brunnauer, P.H. Emmett, E. Teller, J. American Chemical Society, 60 (1938) 309.
[18] P.B. Balbuena, K.E. Gubbins, Theoretical Interpretation of Adsorption Behavior of Simple Fluids in Slit Pores, Langmuir, 9 (1993) 1801-1814.
[19] S.W. Ui, S.J. Lim, S.H. Lee, S.C. Choi, Control of the size and morphology of nano-size silica particles using a sodium silicate solution, Journal of Ceramic Processing Research, 10 (2009) 553-558.